JOM, Vol. 71, No. 7, 2019
https://doi.org/10.1007/s11837-019-03529-1

Spent Lead-Acid Battery Recycling via Reductive Sulfur-Fixing Smelting and Its Reaction Mechanism in the $PbSO_4$-Fe_3O_4-Na_2CO_3-C System

YUN LI,[1,2] SHENGHAI YANG,[1] PEKKA TASKINEN,[2] JING HE,[1] YONGMING CHEN,[1,4] CHAOBO TANG,[1,5] YUEJUN WANG,[3,6] and ARI JOKILAAKSO[1,2,7]

1.—School of Metallurgy and Environment, Central South University, Changsha 410083, China. 2.—Department of Chemical and Metallurgical Engineering, Aalto University, 02150 Espoo, Finland. 3.—Department of Ecology and Resources Engineering, Hetao College, Bayannur 015000, China. 4.—e-mail: csuchenyongming@163.com. 5.—e-mail: chaobotang@163.com. 6.—e-mail: thirtythree61@aliyun.com. 7.—e-mail: ari.jokilaakso@aalto.fi

An innovative and environmentally friendly lead-acid battery paste recycling method is proposed. The reductive sulfur-fixing recycling technique was used to simultaneously extract lead and immobilize sulfur. SO_2 emissions and pollution were significantly eliminated. In this work, the detailed lead extraction and sulfur-fixing mechanisms in the $PbSO_4$-Fe_3O_4-Na_2CO_3-C system were investigated thermodynamically and experimentally, and the phase transformation and microstructural evolution processes characterized. In addition, a series of bench-scale pilot experiments were carried out to confirm the feasibility of the technique. The results show that the lead extraction and sulfur-fixing reactions followed the shrinking unreacted-core model. The recycling products were separated into three distinct layers: slag, matte, and crude lead bullion. Primary recoveries of 96.2% for lead and 98.9% for sulfur were obtained. The purity of the crude lead bullion was 98.6 wt.%. Sulfur was fixed in the solidified matte as FeS and $NaFeS_2$.

INTRODUCTION

Spent lead-acid batteries (LABs) are widely scrapped from automobiles and electric bicycles in urban areas. The reported amounts of scrap LAB annually in China total more than 2.6 million metric tons.[1,2] LABs are a solid waste and classified as hazardous materials in many countries. Their disposal has become a significant environmental concern.[3] Recycling and reuse of LABs are attracting great attention from both the public and materials processing industry. At the same time, the depletion of high-quality lead ores resulting in rising extraction costs presents critical challenges for the lead extractive metallurgical industry. As a result, scrap LABs have become a significant secondary lead source worldwide.[1] Secondary lead produced by recycling is gradually dominating the world's lead market.[4] Typically, a spent LAB consists of four components: waste electrolyte (11–30%), polymeric materials (22–30%), lead alloy grids (24–30%), and lead paste (30–40%). Of these, lead paste is the most difficult part to deal with.[5] However, it is a high-quality secondary lead-bearing material. Around 80–85% of the total secondary lead is recycled from lead paste.[6]

Currently, the worldwide LAB recycling technology can be divided into traditional routes such as pyrometallurgy and hydrometallurgy, and advanced approaches including electrowinning,[7] biological techniques,[8,9] and vacuum methods.[5] Pyrometallurgy is presently the predominant route worldwide for recycling LAB,[10] in which high-temperature treatment of spent LABs in a blast, electric, reverberatory, or rotary furnace without pre-desulfurization is employed.[11,12] In the hydrometallurgical process,[13,14] a pre-desulfurization step[15] is necessary. Na_2CO_3, NaOH, and K_2CO_3 solutions or citric acid and citrate salts are usually adopted as desulfurization reagents. However, the

 (Published online May 16, 2019)

treatment of spent LABs involves a potential health and environmental risk.[16,17] At the same time, existing LAB pyrometallurgical processes operated at high temperatures are usually associated with high atmospheric emissions, since dioxins, chloride compounds, and mercury can be generated in the process. Meanwhile, hydrometallurgical processes are accompanied by laborious procedures, generation of large amounts of problematic waste water, and high electricity consumption.[18] As a result, the stringent environmental requirements are increasingly difficult to meet with current pyro- and hydrometallurgical recycling technologies. Therefore, the lead industry is keen to seek advanced technologies[19] which are more economical, minimize environmental pollution,[20] and reduce energy usage and production costs.

In this article, an innovative and environmentally friendly lead-acid battery paste recycling method is proposed. The reductive sulfur-fixing[21–23] technique was used to simultaneously extract lead and immobilize sulfur. This novel technique is distinguished from conventional pyrometallurgy techniques such as oxidizing matte smelting and reductive smelting by the use of a reducing atmosphere in the processing combined with sulfur transformation and fixation as a sulfide matte. Iron-containing wastes are also employed as sulfur-fixing agents to immobilize sulfur as FeS. The smelting products obtained contain three products, namely crude metal bullion, matte, and slag. The novelty of this process is the treatment of various iron/lead-bearing wastes, SO_2-free sulfur fixation, a much shorter flowsheet, absence of harmful byproducts, and wide adaptability for different secondary materials.[12] This work investigated the detailed lead extraction and sulfur-fixing mechanisms in the $PbSO_4$-Fe_3O_4-Na_2CO_3-C system, thermodynamically and experimentally. The phase transformations and microstructural evolution processes were characterized, and the lead extraction and sulfur-fixing reaction mechanisms proposed. Furthermore, bench-scale experiments were carried out to confirm the feasibility and reliability of the new technique.

EXPERIMENTAL PROCEDURES

Materials

In the reaction mechanism investigation, $PbSO_4$, Na_2CO_3, Fe_3O_4, and carbon powder with purity of ≥ 99% were employed to ensure high experimental accuracy. In the batch tests, lead paste separated from LAB scrap was used as raw material. Hematite and coke obtained from Jiuquan Iron & Steel Co., Ltd., Gansu, China were applied as sulfur-fixing agent and reductant, respectively. Their chemical compositions were analyzed by inductively coupled plasma-atomic emission spectrometry (ICP-AES, PerkinElmer, Optima 3000, Norwalk, USA) and are shown in Supplementary Table S-I (Online Supplementary Material). The phase compositions of the lead paste and hematite were characterized by x-ray diffraction (XRD) analysis (D/max 2550PC, Rigaku Co., Ltd., Japan). The results are presented in Supplementary Fig. S-1, showing that the lead paste comprised 56.3% $PbSO_4$, 18.9% PbO_2, 13.7% Pb, and 11.1% PbO. Lead sulfate (anglesite) is the main substance in the lead paste. Hematite mainly contains Fe_2O_3 and $(Mg,Al)_6(Si,Al)_4O_{10}(OH)_8$, SiO_2, and $Ca(Al,Si)_2O_4$.

Methods

$PbSO_4$ was selected as a model compound in the reaction mechanism investigation, since it is the major as well as the most difficult component to deal with in spent lead paste. At the same time, to reveal the reaction paths that may take place in each raw material component, the $PbSO_4$-Fe_3O_4-Na_2CO_3-C system was divided into the $PbSO_4$-Na_2CO_3, $PbSO_4$-Na_2CO_3-C, $PbSO_4$-Fe_3O_4, and $PbSO_4$-Fe_3O_4-C subsystems. The specimens were mixed carefully and pressed uniaxially under 15 MPa into cylindrical samples of 10 mm diameter. Each specimen was placed in an alumina crucible and pushed slowly into the constant-temperature zone of a horizontal tube furnace (Supplementary Fig. S-2). The temperature was measured using a Pt-Rh thermocouple and controlled using a SHIMADEN SR25 intelligent temperature controller (accuracy ± 1°C). Nitrogen with purity of 99% was applied as protective gas in the reaction mechanism investigations. The N_2 gas flow during the reaction was fixed at 0.5 L/min. After the preset smelting time, the sample was removed rapidly from the furnace and quenched in liquid nitrogen.

In the bench-pilot confirmation experiments, 2000 g LAB paste was mixed thoroughly with a desired proportion of hematite, coke, Na_2CO_3, and other fluxes (CaO and SiO_2). The specimen was loaded into an alumina crucible and put into a chamber furnace. After the required smelting time, the sample was taken out and cooled down at room temperature. Next, the crucible was broken to carefully separate and weigh the end products obtained, i.e., crude lead, ferrous matte, and slag. Each product was prepared for ICP-AES analysis. The direct recovery rate of Pb (η) and the sulfur-fixing rate (γ) were calculated based on Eqs. 1 and 2, respectively:

$$H = \frac{\text{Mass of Pb in the crude lead}}{\text{Mass of Pb in the initial feed materials}} \times 100\% \quad (1)$$

$$\gamma = \frac{\text{Mass of sulfur in the condensed solid smelting products}}{\text{Mass of sulfur in the initial feed materials}} \times 100\% \quad (2)$$

The phases and microstructure of the samples were characterized by XRD using Cu K_α radiation and scanning electron microscope with energy-

dispersive spectroscopy (SEM–EDS, Carl Zeiss LEO 1450, Germany; EDS, INCA Wave 8570, Oxford Instruments, UK). XRD data were collected in the 2θ range from 10° to 80° in steps of 1°. The recorded patterns were evaluated using the PDF-2 powder XRD database.[24] Samples for SEM–EDS analysis were mounted in epoxy resin and polished using conventional metallographic grinding and polishing techniques.

THERMODYNAMIC CALCULATIONS

Figure 1 illustrates the equilibrium compositions of the $PbSO_4$-Fe_3O_4-Na_2CO_3-C reaction system for different carbon additions as simulated using HSC Chemistry software, version 9.2.6, and its database;[25] the phase diagrams of the Al_2O_3-SiO_2-CaO-10 wt.%Na_2O and Fe-Fe_3O_4-FeS systems were calculated using MTDATA version 6.0[26] and MTOX database 8.2.[27] Figure 1a suggests that, without carbon addition, $PbSO_4$ prefers to react with Na_2CO_3 to produce Na_2SO_4 and PbO, even below 200°C. As the temperature is increased above 500°C, some PbO decomposes to metallic lead. In a weakly reductive atmosphere, as shown in Fig. 1b, $PbSO_4$ is reduced to PbS. At the same time, as the temperature increases, PbS prefers to react further with Fe_3O_4, instead of Na_2CO_3, generating metallic Pb and FeS. However, when the temperature reaches around 630°C, Na_2CO_3 gradually reacts with FeS as well as PbS. Thus, the amounts of Pb, Na_2S, and Fe_3O_4 products increase, while those of PbS, Na_2CO_3, and FeS decrease. However, some PbS remains due to insufficient addition of carbon.

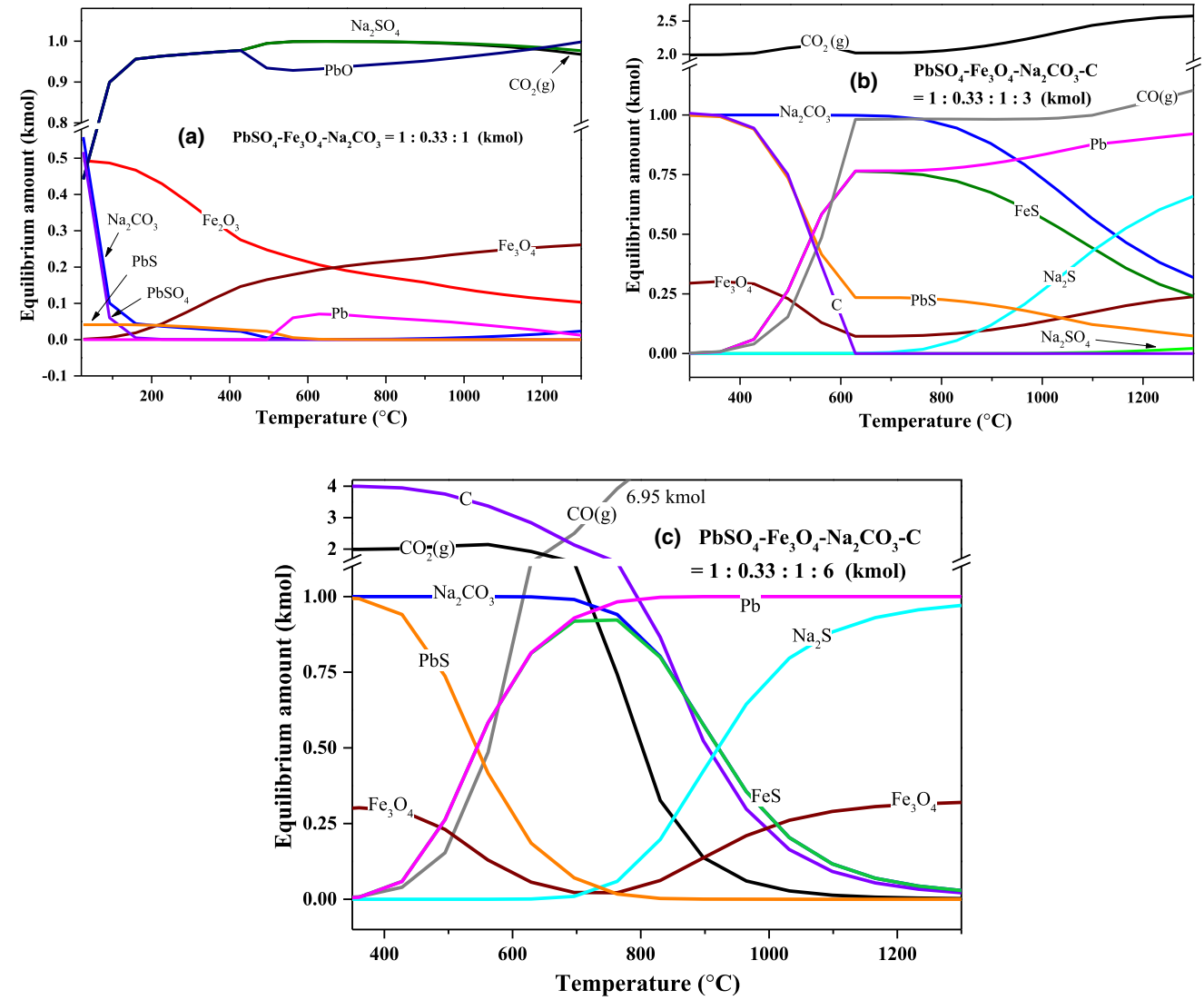

Fig. 1. Equilibrium compositions (a)–(c) of the $PbSO_4$-Fe_3O_4-Na_2CO_3-C reaction system calculated for different carbon additions; data taken from HSC 9.2.6 and its database;[25] and liquidus contour diagrams of (d) the Al_2O_3-SiO_2-CaO-10 wt.%Na_2O system and (e) the Fe-Fe_3O_4-FeS system calculated using MTDATA version 6.0 and MTOX database 8.2.[27]

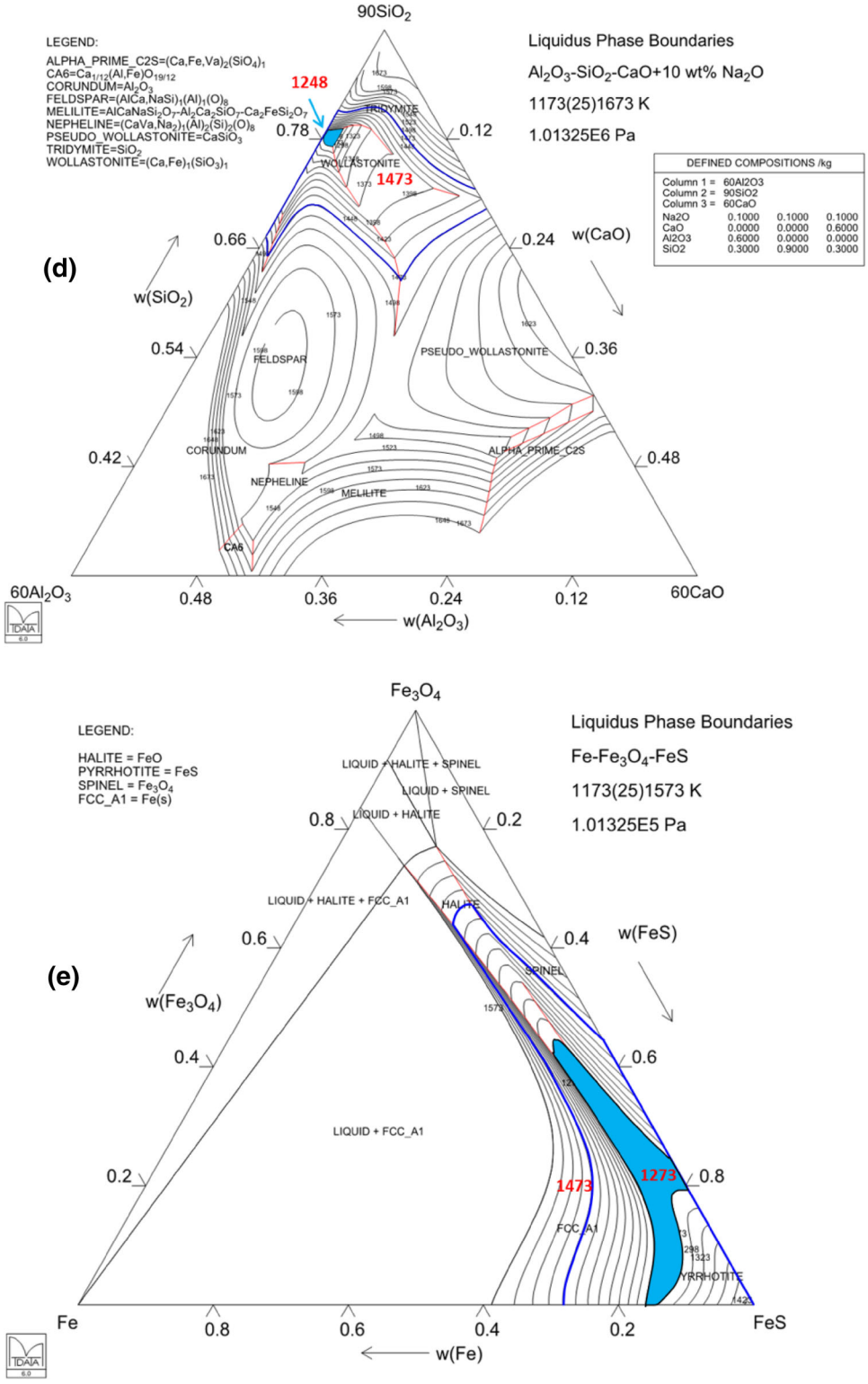

Fig. 1. continued.

Figure 1c indicates that, at equilibrium conditions, all the lead can be extracted from $PbSO_4$ and PbS before 800°C when the carbon addition is sufficient. However, when the temperature is increased from 700°C to 800°C, the equilibrium amount of FeS remains steady while the amounts of metallic Pb and Na_2S increase and, at the same time, those of Na_2CO_3 as well as PbS decrease. This indicates that Na_2CO_3 is partly involved in the lead

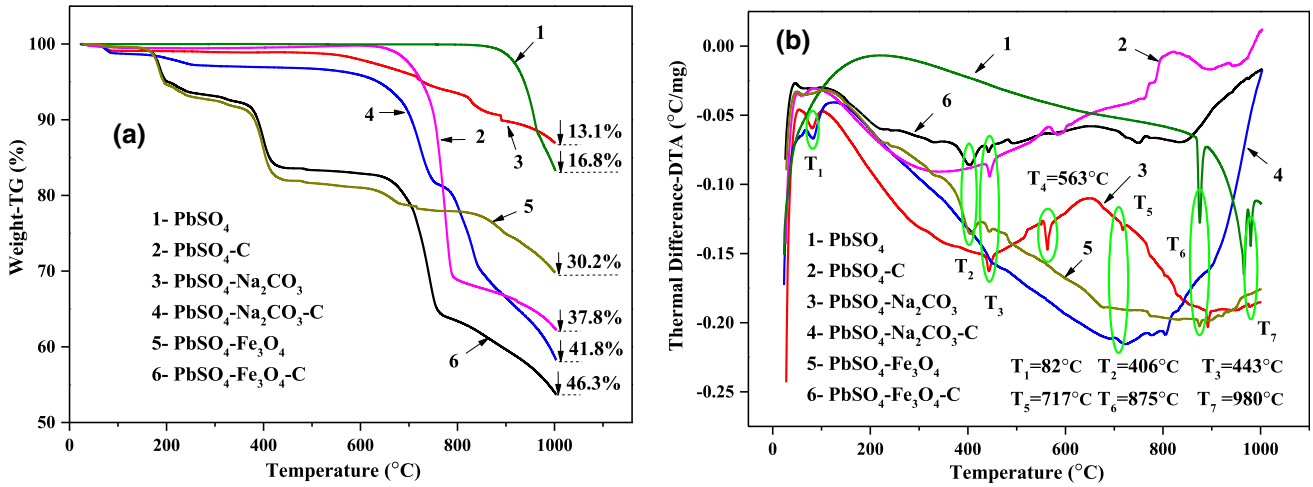

Fig. 2. Thermogravimetric behavior in different $PbSO_4$-Fe_3O_4-Na_2CO_3-C subsystems (mole ratio 3:1:3:18): (a) TG curves, (b) DTA curves.

extraction reactions from PbS. When the temperature exceeds 800°C, some FeS will also react with Na_2CO_3 to generate Na_2S and Fe_3O_4.

The above thermodynamic equilibrium composition calculations reveal that, in the absence of a reducing agent and below 200°C, $PbSO_4$ prefers to react with Na_2CO_3 rather than Fe_3O_4 to generate PbO and Na_2SO_4. Once the temperature is increased and the atmosphere is sufficiently reducing, $PbSO_4$ will be reduced to PbS. At that point, PbS will prefer to react with Fe_3O_4 rather than Na_2CO_3 to produce FeS and PbO. When the temperature exceeds 800°C, the excess Na_2CO_3 will continue to react with FeS. Thus, the sulfur transfers from the initial $PbSO_4$ to PbS and then FeS, and finally to Na_2S. As a result, the presence of Na_2CO_3, and a reductant as well as sulfur-fixing agent Fe_3O_4, can ensure efficient sulfur fixation and lead extraction at both low and high temperature. No gaseous SO_2 or SO_3 is generated throughout the whole reaction process. All lead can thus be extracted from $PbSO_4$ and PbS.

The phase diagrams of the Al_2O_3-SiO_2-CaO-10 wt.%Na_2O system shown in Fig. 1d indicate that the first liquid slag appeared below around 975°C (1248 K), surrounded by liquid wollastonite [(Ca,Fe)SiO_3], tridymite (SiO_2), and feldspar [(AlCa,NaSi)AlO_8]. At that point, PbS, FeS, metallic Pb, Na_2SO_4, and Na_2S were generated in the smelting system, as shown in Fig. 1a–c. They stayed in liquid form, together with the remaining Fe_3O_4 and liquid Na_2CO_3. As the temperature was increased further, more liquid was formed from (Ca,Fe)SiO_3 and other solid smelting materials. When the temperature reached 1200°C (1473 K), more tridymite (SiO_2) and feldspar [(AlCa,NaSi)AlO_8] also dissolved in the melt, and the liquid slag region expanded.

Figure 1e further reveals that pyrrhotite FeS melts may come into contact with spinel Fe_3O_4, halite FeO, or/and FCC-A1 Fe before 1000°C (1273 K). A eutectic iron sulfide–oxide liquid appeared and gradually expanded along with the temperature. At 1200°C (1473 K), FeS was in liquid form. This promoted the generation of FeS and its settling from the smelting system as a separate sulfide melt layer.

RESULTS AND DISCUSSION

Thermogravimetric Behavior of $PbSO_4$-Fe_3O_4-Na_2CO_3-C Mixtures

The thermogravimetric behavior of the reactants and their mixtures was characterized using a thermogravimetric analyzer (TG–DTA, STA 494 F3; Netzsch, Germany) at heating rate of 10°C/min in N_2 flow of 100 mL/min, from 25 to 1000°C. The results are shown in Fig. 2.

It can be observed from Fig. 2a that the weight loss in the $PbSO_4$-C, $PbSO_4$-Na_2CO_3-C, and $PbSO_4$-Fe_3O_4-C subsystems was greater than that in the $PbSO_4$, $PbSO_4$-Fe_3O_4, and $PbSO_4$-Na_2CO_3 subsystems. This implies that the presence of carbon promoted the conversion of $PbSO_4$. Figure 2b further illustrates that T_1 (around 82°C) is associated with loss of crystallographic water from Na_2CO_3. T_2 (406°C) is ascribed to the transformation of Fe_3O_4 into crystal form. T_3 (443°C) corresponds to preliminary decomposition of $PbSO_4$. T_4 (563°C) and T_5 (717°C) are associated with the conversion reactions between $PbSO_4$ and Na_2CO_3. The pronounced endothermic peaks detected at T_6 (around 875°C) can be attributed to further decomposition of $PbSO_4$. The last obvious endothermic peaks recorded at T_7 (around 980°C) are assumed to be linked with the generation of metallic lead.

Experimental Reaction Mechanisms in the $PbSO_4$-Na_2CO_3-C Mixture

The experimental phase transformation paths in the different reaction systems and at different temperatures and reaction times were characterized

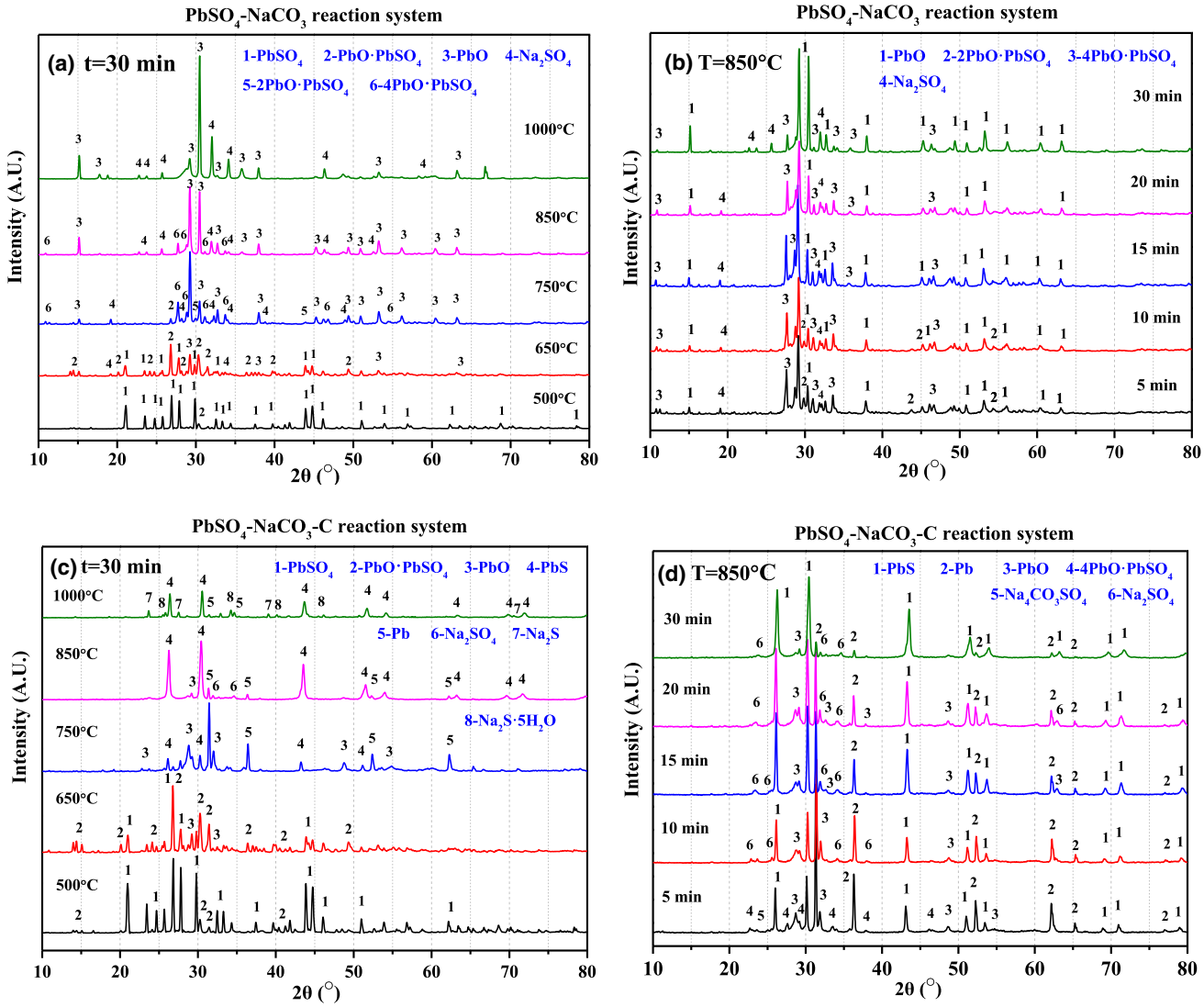

Fig. 3. Phase transformation paths in (a) the $PbSO_4$-Na_2CO_3 (mole ratio 1:1) reaction system at different smelting temperature after 30 min reaction time; (b) the $PbSO_4$-Na_2CO_3 (mole ratio 1:1) reaction system at 850°C for different reaction times; (c) the $PbSO_4$-Na_2CO_3-C (mole ratio 1:1:6) reaction system at different smelting temperatures after 30 min reaction time; (d) the $PbSO_4$-Na_2CO_3-C (mole ratio 1:1:6) reaction system at 850°C for different reaction times.

by XRD and SEM–EDS analyses. The results for the $PbSO_4$-Na_2CO_3-C system are shown in Fig. 3. It was observed that the reactions between $PbSO_4$ and Na_2CO_3 took place below 650°C. PbO and Na_2SO_4 were detected at 650°C within a 30-min duration. At the same time, when the temperature was increased, more intermediate products were detected, e.g., $PbO{\cdot}PbSO_4$, $2PbO{\cdot}PbSO_4$, and $4PbO{\cdot}PbSO_4$. This indicates that the reactions between $PbSO_4$ and Na_2CO_3 are a multistage process and follow the shrinking unreacted-core model. The unreacted $PbSO_4$ core is surrounded by liquid Na_2CO_3. The products xPbO·$PbSO_4$ (x = 1, 2, or 4) form a boundary layer. When the temperature exceeded 1000°C, the reactions were completed and the final products were stable in PbO and Na_2SO_4. No metallic Pb was detected due to the absence of reductant. These results agree well with the thermodynamic calculations presented in Fig. 1. Figure 3b further reveals that the exchange reactions between $PbSO_4$ and Na_2CO_3 favorably occur at 850°C quickly, within as little as 5 min. Thus, SO_3 in $PbSO_4$ was transformed and fixed to Na_2SO_4, instead of being emitted to the furnace atmosphere. The presence of Na_2CO_3 inhibited self-decomposition of $PbSO_4$.

Once a reductant was present, as shown in Fig. 3c and d, $PbSO_4$ was reduced to PbS when the temperature was higher than 750°C. Metallic Pb was also detected. This implies that PbO had been reduced by carbon. Furthermore, as the temperature was increased to 1000°C, the stable sodium-bearing product after 30 min reaction time was Na_2S, rather than Na_2SO_4. This indicates that Na_2SO_4 had been reduced to Na_2S. The final products were PbS, Pb, and Na_2S.

The reaction paths in the $PbSO_4$-Na_2CO_3-C system at 850°C after different reaction times, which are illustrated in Fig. 3d, further reveal that the $PbSO_4$ and PbO reduction reactions can occur rapidly. PbS and metallic Pb appeared within 5 min reaction time. The presence of carbon thus changes the reaction paths in the $PbSO_4$-Na_2CO_3 system. Only very weak diffraction peaks of PbO, $Na_4CO_3SO_4$, and Na_2SO_4 were detected in the reaction products. The reduction of $PbSO_4$ to PbS dominated the reaction path at 850°C. The sulfur in $PbSO_4$ would be converted mainly to PbS rather than Na_2SO_4.

Experimental Reaction Mechanisms in the $PbSO_4$-Fe_3O_4-C Mixtures

Figure 4 presents the phase evolutions in the $PbSO_4$-Fe_3O_4-C system. It can be observed in Fig. 4a and b that no reactions took place between $PbSO_4$ and Fe_3O_4 in the absence of reductant, as only a decomposition product, viz. $PbO{\cdot}PbSO_4$ from $PbSO_4$, was detected. With the addition of a reductant, as illustrated in Fig. 4c, below 650°C, $PbSO_4$ was still not involved in any reaction with iron oxide during the first 30 min. However, at 750°C, PbS was detected, and $PbSO_4$ also converted to $PbO{\cdot}PbSO_4$ and further to $2PbO{\cdot}PbSO_4$, and metallic Pb emerged. This implies that, without Na_2CO_3, $PbSO_4$ self-decomposition intensified. As the temperature increased to 850°C, the product after 30 min reaction time consisted of PbS, Pb, and Fe_3O_4. Figure 4d further illustrates that the $PbSO_4$ reduction reactions to PbS could take place instantaneously. $PbSO_4$ disappeared before it was involved in any reaction with Fe_3O_4. FeS did not emerge until 1000°C after 30 min reaction time, and was

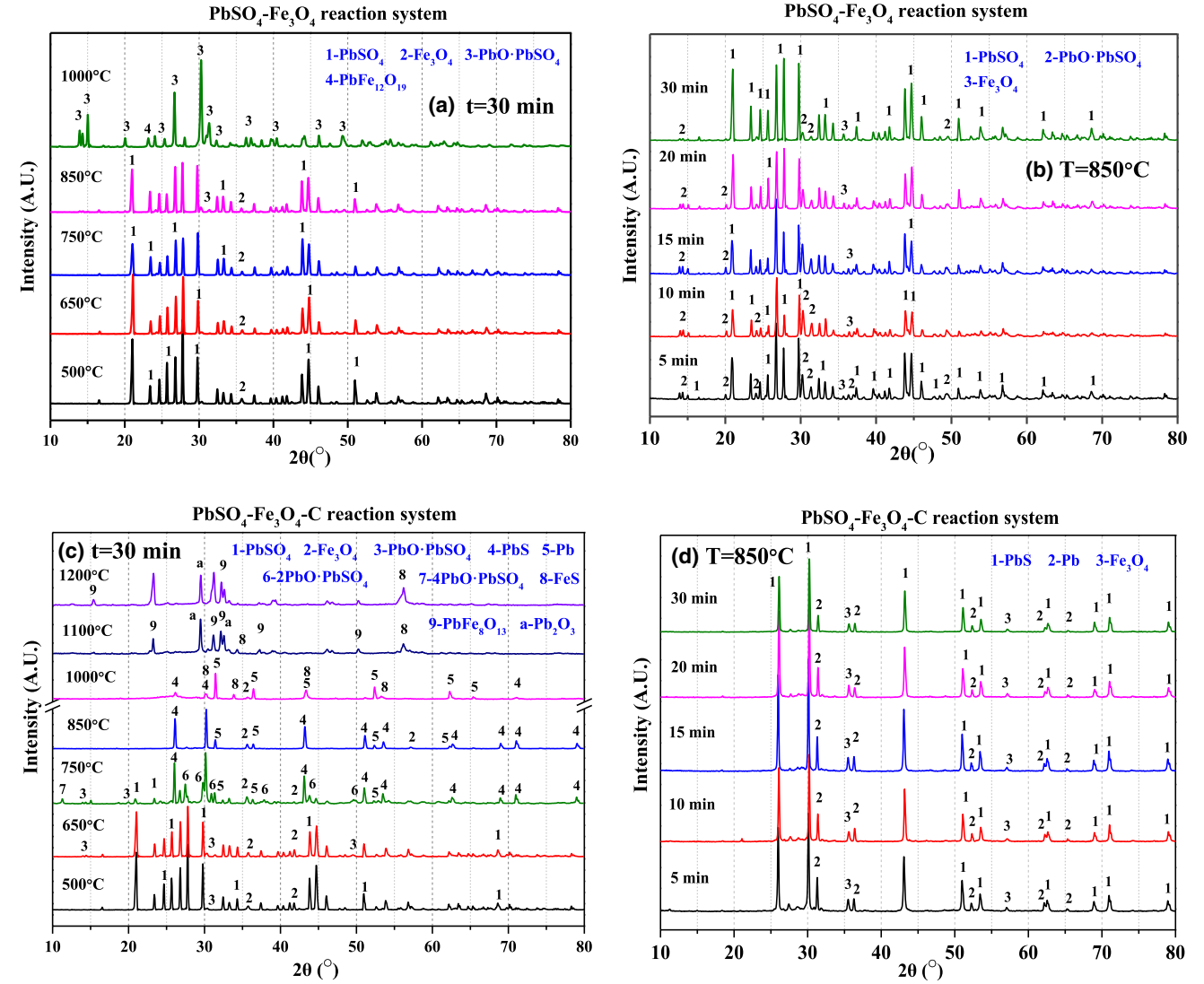

Fig. 4. Phase transformation paths in (a) the $PbSO_4$-Fe_3O_4 (mole ratio 3:1) reaction system at different smelting temperatures after 30 min reaction time; (b) the $PbSO_4$-Fe_3O_4 (mole ratio 3:1) reaction system at 850°C for different reaction times; (c) the $PbSO_4$-Fe_3O_4-C (mole ratio 3:1:18) reaction system at different smelting temperatures after 30 min reaction time; (d) the $PbSO_4$-Fe_3O_4-C (mole ratio 3:1:18) reaction system at 850°C for different reaction times.

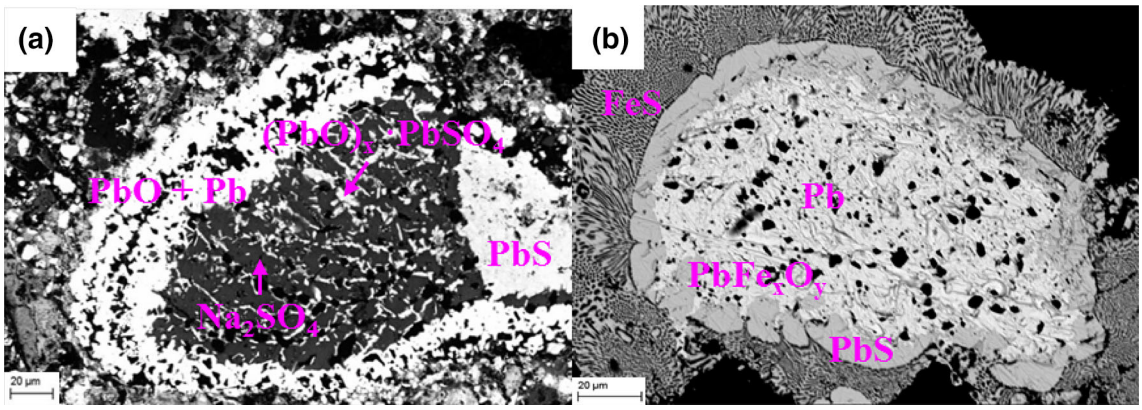

Fig. 5. SEM micrographs of products generated in (a) the $PbSO_4$-Na_2CO_3-C system at 750°C after 30 min reaction and in (b) the $PbSO_4$-Fe_3O_4-C system at 850°C after 5 min reaction.

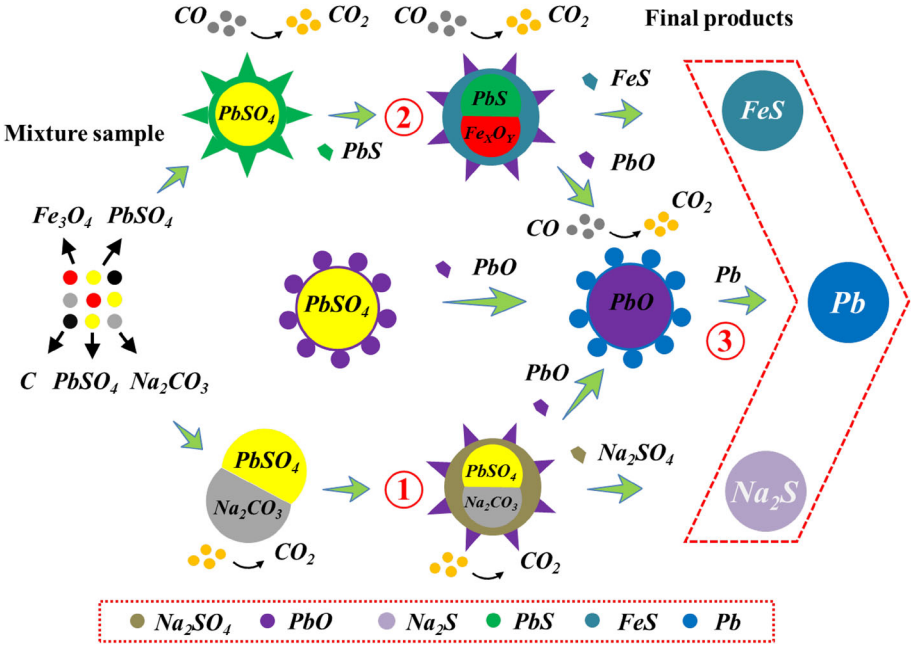

Fig. 6. Phase transformation and microstructural evolution mechanisms during reductive sulfur-fixing recycling process of scrap lead battery paste.

generated by the exchange reactions between PbS and Fe_3O_4. $PbSO_4$ did not directly react with the sulfur-fixing agent, iron oxide. The sulfur-fixation reactions occurred with the help of exchange reactions between $PbSO_4$ and Na_2CO_3, as well as PbS and Fe_3O_4. The reaction mechanism proposed is consistent with the thermodynamic results above.

Microstructural Evolution Mechanisms

Selected samples, produced from simulated smelting systems at different temperatures and reaction times, were further characterized by SEM–EDS analysis. The results are presented in Fig. 5. Figure 5a shows the SEM–EDS results for the $PbSO_4$-Na_2CO_3-C system at 750°C for 30 min reactions. It was observed that $(PbO)_x \cdot PbSO_4$ (x = 1, 2, or 4) was close to Na_2SO_4 particles and a part of $PbSO_4$ had reduced to PbS. Moreover, $PbSO_4$ and Na_2SO_4 were surrounded by PbO and metallic Pb. This confirms that the reactions between $PbSO_4$ and Na_2CO_3 follow the shrinking unreacted-core model. $PbSO_4$ first reacts with Na_2CO_3 to generate Na_2SO_4 and PbO. Na_2CO_3 surrounds and gradually "erodes" the $PbSO_4$ unreacted core, then the $PbSO_4$ core is disintegrated by molten Na_2SO_4. At the same time, the reaction product PbO gradually diffuses out from the unreacted $PbSO_4$ core.

Figure 5b illustrates the SEM–EDS results for the $PbSO_4$-Fe_3O_4-C system at 850°C after 5 min reaction time. It reveals that PbS was surrounded by FeS. Metallic Pb was located in the center of the PbS particle. A $PbFe_xO_y$ boundary layer was detected between the metallic Pb and PbS layers. This demonstrates that the reactions between PbS and Fe_xO_y also follow the shrinking unreacted-core model. A possible phase transformation and

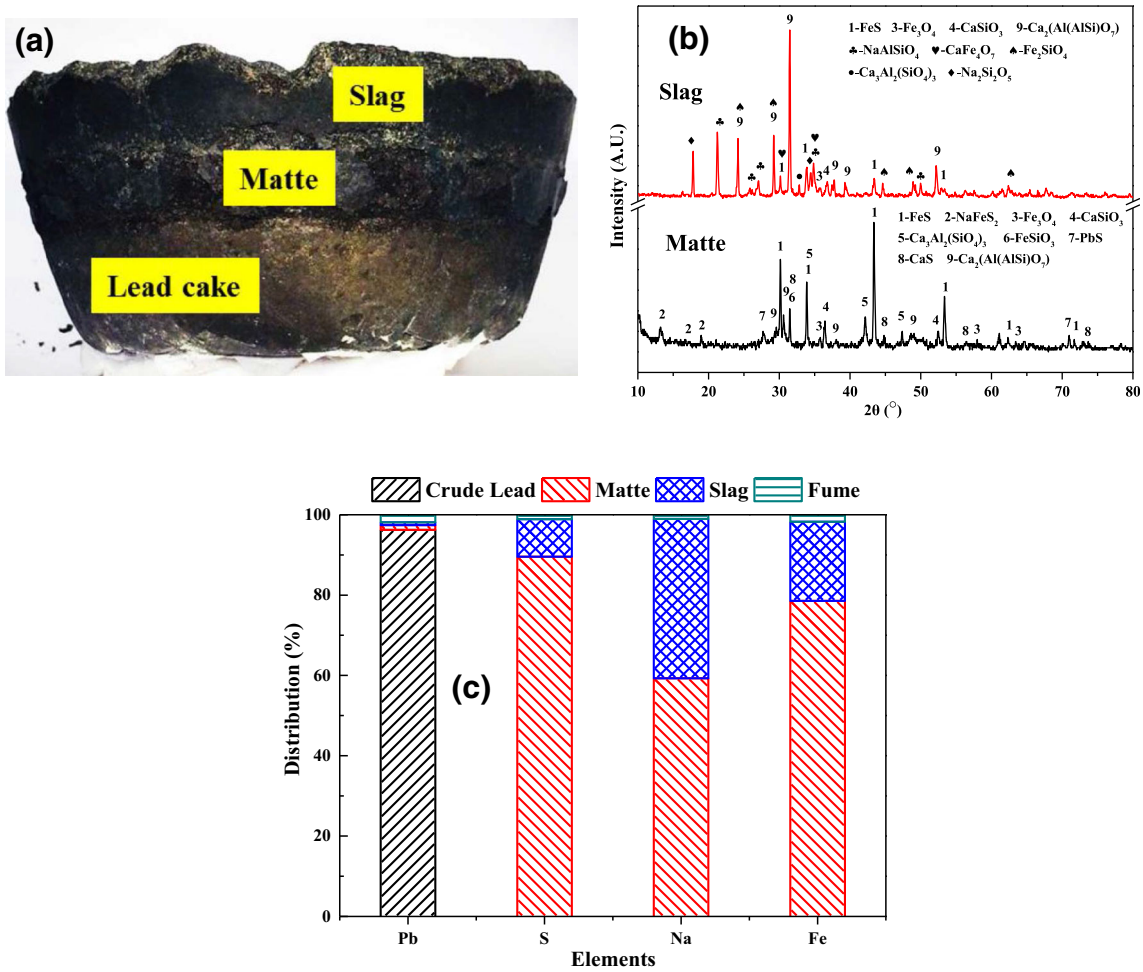

Fig. 7. (a) Macrograph of smelting products in bench-scale pilot experiments; (b) XRD patterns of matte and slag; (c) element distribution behavior ($W_{\text{lead paste}}$: W_{hematite} : $W_{Na_2CO_3}$: W_{coke} = 1800 g:360 g:72 g: 216 g. FeO/SiO_2 = 1.3, CaO/SiO_2 = 0.4, 1200°C, 1.5 h).

microstructural evolution mechanism for the entire $PbSO_4$-Na_2CO_3-Fe_3O_4-C reaction system is summarized and presented graphically in Fig. 6.

Confirmation Experiments and Characterization of Products

Two bench-scale pilot confirmation experiments with 1800 g lead paste were carried out to determine the reliability of this novel process under the following conditions: $W_{\text{lead paste}}$: W_{hematite} : $W_{Na_2CO_3}$: W_{coke} = 100 g:20 g:4 g:12 g. FeO/SiO_2 = 1.3, CaO/SiO_2 = 0.4, smelting temperature of 1200°C, and smelting time of 1.5 h. A physical macrograph and corresponding XRD patterns of the smelting products are presented in Fig. 7a and b. It can be observed that three products were obtained, visibly separated as distinct layers by settling, i.e., slag, ferrous matte, and crude lead bullion. The chemical compositions of the different products obtained and the element distribution behavior is presented in Fig. 7c and Table S-II (Supplementary Material).

The above results validate the reductive sulfur-fixing technique as being experimentally feasible for recycling LAB paste. More than 96.2% of the lead and 98.9% of the sulfur (89.6% in the matte and 9.3% in the slag) in the raw materials were extracted and fixed within 1.5 h at 1200°C. Crude lead bullion with purity of 98.6 wt.% Pb was obtained. The lead content in the matte and slag were 2.6 wt.% and 0.5 wt.%, respectively. The major constituent in the matte was FeS. Some CaS, Fe_3O_4, and unreacted PbS as well as entrained gangue materials such as $Ca_3Al_2(SiO_4)_3$, $FeSiO_3$, $Ca_2(Al(AlSi)O_7$, and $CaSiO_3$ were also detected. The solidified slag comprised $Ca_2(Al(AlSi)O_7$, Fe_2SiO_4, $CaFe_4O_7$, $NaAlSiO_4$, $Na_2Si_2O_5$, $CaSiO_3$, Fe_3O_4, $Ca_2Al_2(SiO_4)_3$, and some entrained FeS.

The matte and slag that were obtained were further characterized by SEM–EDS analysis. The results are shown in Fig. 8. Figure 8a–d shows that, in the matte, mackinawite mineral FeS was bonded to magnetite Fe_3O_4. Sodium iron sulfide $NaFeS_2$ and galena PbS filled the gaps between the

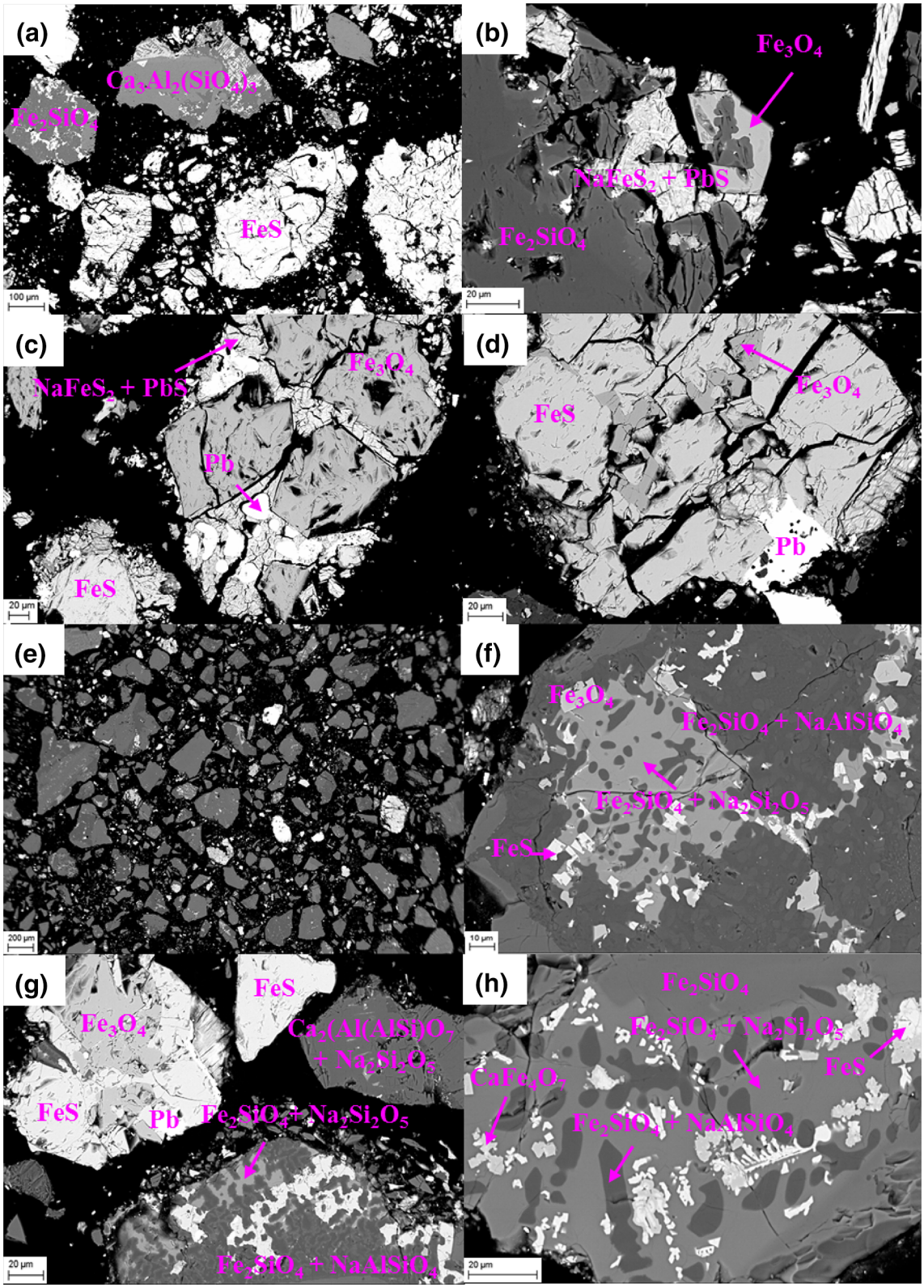

Fig. 8. SEM micrographs of the experimental bench-scale pilot products; (a)–(d) matte; (e)–(h) slag.

magnetite minerals. Metallic Pb was detected, embedded in the FeS and $NaFeS_2$ minerals. In the slag, as shown in Fig. 8e–h, sodium aluminosilicate ($NaAlSiO_4$) and sodium disilicate ($Na_2Si_2O_5$) dissolved in fayalite Fe_2SiO_4 and gehlenite $Ca_2(Al(AlSi)O_7$. Mackinawite FeS was entrained in the magnetite Fe_3O_4 and calcium iron oxide $CaFe_4O_7$ minerals, and magnetite had separated out from the fayalite matrix. These results agree well with the thermodynamic phase diagram calculations above.

CONCLUSION

Effective lead extraction from LAB paste by a reductive sulfur-fixing recycling technique was shown to be feasible, thermodynamically and experimentally. The reaction mechanism investigations revealed that the presence of Na_2CO_3 helped to transform SO_3 from $PbSO_4$ to Na_2SO_4 at low temperatures and in weakly reductive atmospheres. This ensures the conservation of sulfur in the smelting system without emitting gaseous SO_2 to the atmosphere. Once the atmosphere was sufficiently reductive, $PbSO_4$ was reduced to PbS. Thus, the sulfur-fixing agent Fe_3O_4 reacted with PbS to transfer sulfur to iron matte. Finally, metallic lead was extracted from PbO, and sulfur was fixed as FeS and $NaFeS_2$. The lead extraction and sulfur-fixing reactions followed the shrinking unreacted-core model. Furthermore, bench-scale experiments using lead paste as raw material validated the fact that three recycling products were obtained: slag, matte, and crude lead bullion. More than 96.2% of the lead and 98.9% of the sulfur in the raw materials were extracted and fixed. The purity of the crude lead bullion was 98.6% Pb. The lead content in the matte and slag was decreased to 2.6% and 0.5% in the one-step treatment, respectively. This new process can be used for cotreating various iron-containing solid wastes and residues, and for comprehensive recycling of a variety of valuable metals compatible with iron matte and metallic lead.

ACKNOWLEDGEMENTS

Open access funding provided by Aalto University. This work is supported by the Specialized Research Project of Guangdong Provincial Applied Science and Technology, China (Grant No. 2016B020242001), Hunan Provincial Science Fund for Distinguished Young Scholars, China (Grant No. 2018JJ1044), National Natural Science Foundation of China (Grant Nos. 51234009 and 51604105), CMEco by Business Finland (Grant No. 2116781), National Natural Science Foundation for Less Developed Regions of China (Grant No. 51664013), Program for Young Talents of Science and Technology in Universities of the Inner Mongolia, China (Grant No. NJYT-17-B35), and Bayannur Science and Technology Project from Bayannur Bureau of Science and Technology for Wang Yuejun, China (Grant No. K201509).

OPEN ACCESS

ELECTRONIC SUPPLEMENTARY MATERIAL

The online version of this article (https://doi.org/10.1007/s11837-019-03529-1) contains supplementary material, which is available to authorized users.

REFERENCES

1. Q. Zhang, *Int. J. Electrochem. Sci.* 8, 6457 (2013).
2. X. Tian, Y. Wu, Y. Gong, and T. Zuo, *Waste Manag. Res.* 33, 986 (2015).
3. Z. Sun, H. Cao, X. Zhang, X. Lin, W. Zheng, G. Cao, Y. Sun, and Y. Zhang, *Waste Manag.* 64, 190 (2017).
4. T.W. Ellis and A.H. Mirza, *J. Power Sources* 195, 4525 (2010).
5. D. Lin and K. Qiu, *Waste Manag.* 31, 1547 (2011).
6. R.A. Huggins, *Lead-Acid Batteries* (US: Springer, 2016).
7. D. Andrews, A. Raychaudhuri, and C. Frias, *J. Power Sources* 88, 124 (2000).
8. J. Weijma, K. de Hoop, W. Bosma, and H. Dijkman, *Biotechnol. Prog.* 18, 770 (2002).
9. A. Schröder-Wolthoorn, S. Kuitert, H. Dijkman, and J.L. Huisman, *Hydrometallurgy* 94, 105 (2008).
10. M.A. Kreusch, M.J.J.S. Ponte, H.A. Ponte, N.M.S. Kaminari, C.E.B. Marino, and V. Mymrin, *Resour. Conserv. Recycl.* 52, 368 (2007).
11. X. Zhang, L. Li, E. Fan, Q. Xue, Y. Bian, F. Wu, and R. Chen, *Chem. Soc. Rev.* 47, 7239 (2018).
12. Y. Li, S. Yang, W. Lin, P. Taskinen, J. He, Y. Wang, J. Shi, Y. Chen, C. Tang, and A. Jokilaakso, *Minerals* 9, 119 (2019).
13. R. Prengaman and A. Mirza, *Lead-Acid Batteries for Future Automobiles* (Amsterdam: Elsevier, 2017), p. 575.
14. E. Kim, J. Roosen, L. Horckmans, J. Spooren, K. Broos, K. Binnemans, K.C. Vrancken, and M. Quaghebeur, *Hydrometallurgy* 169, 589 (2017).
15. A. Singh and P. Karandikar, *Microsyst. Technol.* 23, 2263 (2017).
16. T.J. Van der Kuijp, L. Huang, and C.R. Cherry, *Environ. Health* 12, 61 (2013).
17. X. Tian, Y. Wu, P. Hou, S. Liang, S. Qu, M. Xu, and T. Zuo, *J. Clean. Prod.* 144, 142 (2017).
18. A.D. Ballantyne, J.P. Hallett, D.J. Riley, N. Shah, D.J. Payne, and R. Soc, *Open Sci.* 5, 171368 (2018).
19. Y. Li, S. Yang, P. Taskinen, J. He, F. Liao, R. Zhu, Y. Chen, C. Tang, Y. Wang, and A. Jokilaakso, *J. Clean. Prod.* 217, 162 (2019).
20. M. L. Jaeck, in *Primary and Secondary Lead Processing: Proceedings of the International Symposium on Primary and Secondary Lead Processing, Halifax, Nova Scotia, Canada, August 20–24*, Elsevier, Amsterdam (2013), p. 113.
21. Y. Hu, C. Tang, M. Tang, Y. Chen, J. Yang, S. Yang, and J. He, *China Nonferr. Metall.* 43, 75 (2014).
22. L. Ye, C. Tang, Y. Chen, S. Yang, J. Yang, and W. Zhang, *J. Clean. Prod.* 93, 134 (2015).
23. Y. Li, C. Tang, Y. Chen, S. Yang, L. Guo, J. He, and M. Tang, in *8th International Symposium on High-Tempera-*

ture Metallurgical Processing, TMS, San Diego, CA, US, March 23–26 (Springer, Cham, 2017), p. 767.
24. B. Toby, *J. Appl. Crystallogr.* 38, 1040 (2005).
25. A. Roine, *HSC Chemistry for Windows, vers. 9.2.6* (Outotec Research, Pori, Finland, 2019). www.hsc-chemistry.com.
26. *MTDATA ver. 8.2.* (NPL, Teddington, 2015). https://mtdata.com.au/.
27. J. Gisby, P. Taskinen, J. Pihlasalo, Z. Li, M. Tyrer, J. Pearce, K. Avarmaa, P. Björklund, H. Davies, M. Korpi, S. Martin, L. Pesonen, and J. Robinson, *Metall. Mater. Trans. B* 48B, 91 (2017).